
Latent Video Prediction Learns Better World Models

Ali J Alrasheed^{1*} Aryan Yazdan Parast¹ Basim Azam¹ James Bailey² Naveed Akhtar¹
¹The University of Melbourne ²Monash University

Abstract

Self-supervised video models are increasingly framed as world models, yet their evaluation remains largely confined to a single top-1 accuracy score on clean benchmarks. This leaves a major gap in comprehending their potential as world models. We present the first systematic study addressing this gap, analyzing four matched-capacity frontier video foundation models, V-JEPA 2.1, V-JEPA 2, VideoPrism, and VideoMAEv2, across five robustness axes relevant to their deployment as video world models: feature discriminability, corruption robustness, fine-grained discrimination, occlusion robustness, and sensitivity to temporal direction. Our evaluations establish that across all five axes, latent-prediction models form a distinct and consistent profile. They degrade more gracefully under pixel corruption, preserve usable class structure rather than mere geometric stability under occlusion, capture fine-grained physical contact cues without reconstructing pixels, and uniquely encode the arrow of time. These advantages can even survive task adaptation: a frozen V-JEPA 2 backbone with a lightweight attentive probe outperforms a fully fine-tuned VideoMAE and a supervised TimeSformer on corruption and occlusion robustness. Our extensive results offer concrete new evidence in favor of latent prediction for robust world modeling.

1 Introduction

Recent self-supervised video models are increasingly positioned as world foundation models, systems that learn the dynamics of the physical world from observation. The Joint Embedding Predictive Architecture (JEPA) [20] is central to this shift. Rather than reconstructing raw pixels, JEPA learns to predict in a learned latent space, motivated by the hypothesis that latent prediction captures the causal structure of the world more effectively than pixel reconstruction.

What does it mean for such a representation to understand the world? Current practice reduces this question to a single top-1 accuracy score on clean downstream classification benchmarks [3, 21, 27, 29], which remains restrictive in offering insights into the properties a deployed world model must truly possess, e.g., stability under sensor noise and environmental change, tolerance to missing input, fine-grained discrimination between visually similar actions, and an internal sense of temporal order. A comparable evaluation at the level of pretraining objectives also remains missing for such models.

We address this gap through a controlled study of four public video models, V-JEPA 2.1 [21], V-JEPA 2 [3], VideoPrism [29], and VideoMAEv2 [27], spanning the three dominant self-supervised paradigms: latent prediction, contrastive plus masked prediction, and pixel reconstruction. To isolate the pretraining objective, we hold three axes fixed: backbone capacity, evaluation data and protocol, and a classifier probe tuned per encoder to prevent probe mismatch. Remaining factors are fixed by each public release and cannot be equalised without retraining from scratch under a shared compute budget. To test whether frozen representations remain competitive with task-specific optimisation, we additionally compare frozen V-JEPA,2 against an end-to-end fine-tuned VideoMAE [26] and a fully supervised TimeSformer [5].

Through this systematic evaluation across five major experiments that consumed over 1,000 A100 GPU-hours, we uncover the following major intriguing insights:

*Corresponding author: aalrasheed@student.unimelb.edu.au

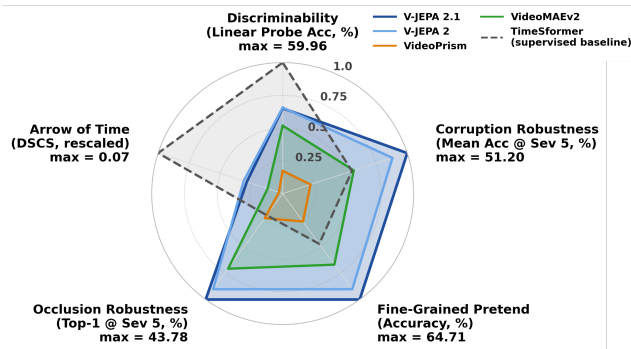


Figure 1: Multi-axis robustness profile of models on Something-to-Something v2 [9]. Each axis shows a normalised score, capturing complementary properties of world models. Higher values are better; raw maxima are annotated. V-JEPA variants are the only models achieving consistently large polygons, indicating balanced strength across the axes. The supervised TimeSformer baseline is competitive on clean metrics but degrades under corruption and occlusion, highlighting that a single top-1 score can mask critical deployment-relevant weaknesses.

- **Latent-prediction models are substantially more robust under pixel corruption.** V-JEPA 2.1 leads on five of six corruption types and shows the slowest accuracy degradation across severities, consistent with the joint-embedding predictive objective discarding surface-level visual variation in favour of higher-order semantic structure.
- **Stable features are not the same as usable features for these model.** Under the most severe spatiotemporal patch dropout, VideoPrism maintains representational similarity above 0.98 yet collapses to 2.7% top-1 accuracy, while V-JEPA 2.1 retains 46.1% on the same clips, showing that cosine similarity alone is a misleading measure of representational stability.
- **Latent prediction captures fine-grained visual cues without reconstructing pixels.** V-JEPA outperforms the pixel-reconstruction baseline on virtually every class of ‘pretend actions’, with the largest margins precisely on high-sensitivity classes whose discriminative signal is the absence of actual physical contact.
- **Latent-prediction models internalise the arrow of time substantially more strongly than the alternatives.** Under video reversal, V-JEPA models flip predictions coherently to semantically antonymous classes such as pushing and pulling, achieving a Directional Semantic Coherence Score (DSCS) several times higher than VideoMAEv2 and VideoPrism.

2 Related work

Video self-supervised learning and world models. Self-supervised learning (SSL) encompasses several paradigms aimed at learning useful representations from unlabeled data. Contrastive methods [7, 10] learn view-invariant features but capture limited temporal dynamics. Generative methods [16, 26] shift the objective to pixel reconstruction, encouraging models to capture the underlying structure of the data. More recently, Joint-Embedding Predictive Architectures (JEPAs) [20] argue that prediction should occur in learned latent spaces rather than pixel space, a philosophy instantiated for images in I-JEPA [2], extended to video in V-JEPA [4], and scaled in V-JEPA 2 [3] to over one million hours of internet video. This philosophy connects to the broader ambition of learning internal world models that support planning and physical reasoning [11, 12, 13, 14, 15]. On the generative side, Cosmos [1] and Genie 2 [23] demonstrate open-weight world foundation models and action-controllable environment generation, respectively. DINO-WM [30] further showed that predicting future states using latent-prediction principle can enable zero-shot planning.

Robustness evaluation. Prior work on image transformers has documented substantial accuracy retention under severe occlusion and distribution shift, attributed to content-dependent global attention rather than texture bias [22, 24], grounded in the corruption benchmarking framework of [17]. Caron et al. [6] further demonstrated that self-supervised ViTs develop emergent segmentation capabilities, establishing that the self-supervised objective shapes structural properties beyond task performance. However, most relevant to latent prediction, Garrido et al. [8] showed that V-JEPA acquires intuitive physics understanding through representation-space masked prediction alone, while pixel-reconstruction models perform near chance on the same benchmarks. Joseph et al. [19] provided the first interpretability study of physics representations inside V-JEPA 2 and VideoMAEv2, finding that latent prediction gives rise to qualitatively different internal organisation. On the temporal axis,

Table 1: Frozen encoders evaluated with a unified attentive probe.

Model	Training Objective
V-JEPA 2.1	Latent prediction
V-JEPA 2	Latent prediction
VideoPrism	Contrastive + mask prediction
VideoMAEv2	Mask prediction

Table 2: Models compared under different training regimes using publicly available checkpoints.

Model	Fine-tuning on SSv2
V-JEPA 2	Attentive-probe only
VideoMAE v1	End-to-end fine-tuned
TimeSformer	Fully supervised

prior work has collectively established that video models frequently rely on static appearance cues and that deeper layers progressively lose temporal order information [25, 18, 28]. Despite this body of work, a comparative evaluation of how distinct video self-supervised paradigms respond to different realistic perturbations remains absent from the literature.

3 Evaluation framework

A representation intended for use as a video world model must do more than classify clean clips correctly. It must remain reliable under sensor noise and environmental change, tolerate missing input, distinguish visually similar actions that differ only in fine physical detail, and capture how a scene evolves over time, including the direction in which events unfold. Rather than establishing a new clean-accuracy ranking, our goal is to characterise how each pretraining paradigm *degrades* along these axes, and whether the choice of objective leaves a measurable structural signature that single-score benchmarks miss. To this end, we hold model capacity, readout protocol, and data distribution fixed across all experiments, varying only the pretraining objective. We describe the models and dataset before summarising the five experiments and the findings.

Models. We compare four publicly available video foundation models at matched ViT-L capacity, each kept frozen and read out through a lightweight attentive probe [2] (Table 1). The four models span the three dominant self-supervised video paradigms: joint-embedding latent prediction (V-JEPA 2.1, V-JEPA 2), contrastive plus masked prediction (VideoPrism), and pixel reconstruction (VideoMAEv2). In Section 9, we additionally run a competitiveness probe (Table 2) that asks whether frozen V-JEPA 2 features remain on par with an end-to-end fine-tuned VideoMAE and a fully supervised TimeSformer trained specifically for the task. This second comparison is restricted to public checkpoints, which dictate the baseline choices included in the evaluations.

Dataset. Because our objective is to measure how performance degrades under controlled perturbations rather than to rank models on a new clean benchmark, the controlled variable is the perturbation, not the data distribution. For our evaluation, what matters is a benchmark whose class structure is rich enough to expose the failure modes of interest. Something-Something v2 (SSv2) [9] meets this requirement. This large-scale dataset comprises over 220,000 videos across 174 fine-grained human-object interaction categories, including visually similar but temporally distinct pairs such as “pushing something left” versus “pushing something right” that force genuine temporal discrimination, and the antonym structure required for the pretend-action and reversal probes. Our extensive evaluation with SSv2 required over 1,000 GPU hours using high-end NVIDIA A100.

Evaluation axes. In our experiments, we probe five complementary axes of representation quality:

- **Feature Discriminability.** Separability of representations on 600 videos drawn from 30 classes (20 videos each), spanning different levels of semantic difficulty.
- **Corruption Robustness.** Classification accuracy under six ImageNet-C corruptions [17] (motion blur, snow, pixelation, impulse noise, brightness, and elastic transform) at three severity levels on a class-balanced set of 500 videos.
- **Fine-Grained Action Discrimination.** Performance on the pretending subset (1,992 videos, 22 classes), where distinguishing real from simulated physical interactions requires sensitivity to fine spatiotemporal contact cues.
- **Occlusion Robustness.** Three spatiotemporal occlusion paradigms at three severity levels on a 1,740-video balanced set spanning 174 classes.
- **Temporal Robustness.** Four temporal disruption paradigms (frame shuffling, reversal, static replacement, and noise injection) on 1,740-video balanced set spanning 174 classes, measuring sensitivity to disrupted order and to the direction of time.

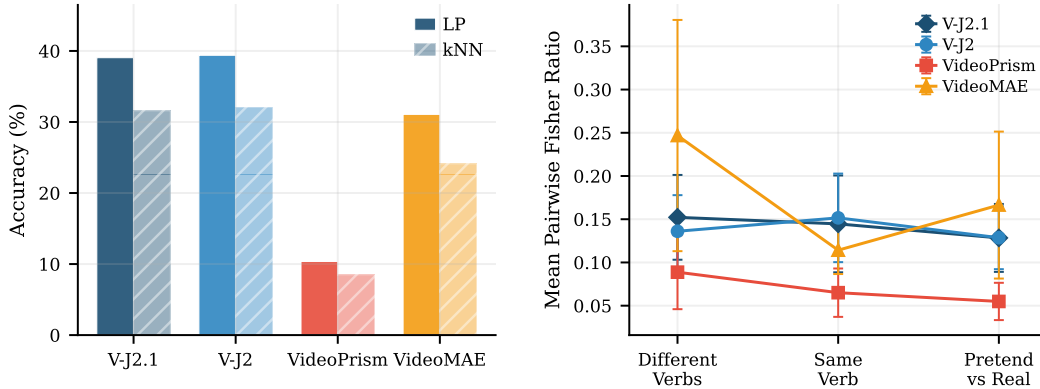


Figure 2: Encoder discriminability on semantically stratified action classes using frozen GAP features (higher is better in both panels). **(Left)** Linear probe and kNN accuracy. **(Right)** Fisher discriminant ratio across three semantic categories ordered by increasing difficulty: *different-verb* (distinct actions, e.g., folding vs. stacking), *same-verb* (shared verb differing only in direction or object, e.g., pushing left-to-right vs. right-to-left), and *pretend-vs-real* (visually near-identical pairs, e.g., pouring vs. pretending to pour). Lines connect category-level means; error bars show standard deviation.

Outline of the results. The sections below report result and analysis following the experiment order listed above: feature discriminability (Section 4), corruption robustness (Section 5), pretend versus real action discrimination (Section 6), occlusion robustness (Section 7), and temporal robustness (Section 8). Section 9 then asks whether the advantages observed for frozen V-JEPA representations survive when the baselines are allowed to fine-tune end-to-end on the same task. The unifying question across all six sections is whether the choice of pretraining objective leaves a measurable structural signature in the base representation that single-score benchmarks miss.

4 Do latent-prediction models produce better representations?

We measure the discriminability of frozen video representations using global average pooled (GAP) features across models in Table 1. The 30 selected action classes are listed in Appendix B, stratified into three tiers of increasing semantic difficulty, i.e., different-verb actions, same-verb actions, and pretend-vs-real, chosen so that successive tiers progressively remove the coarse appearance and motion cues a representation could exploit, isolating progressively finer-grained semantic structure.

V-JEPA models produce the most discriminable representations. Both V-JEPA variants achieve substantially higher linear probe accuracy than VideoMAEv2 and VideoPrism across the semantically stratified action classes - Figure 2 (left). Although VideoMAEv2 attains the highest global Fisher discriminant ratio - Figure 2 (right), this does not translate into superior classification accuracy, indicating that inter-class variance alone is insufficient for linear separability. The gap between linear probe and kNN accuracy is largest for the V-JEPA models (Appendix B, Figure 8), suggesting that their representations encode direction-dependent semantic structure that a learned linear head can exploit more effectively than a nearest-neighbor classifier.

V-JEPA separability is consistent across semantic categories; VideoMAE is not. Per-category Fisher analysis shows that V-JEPA models maintain a almost consistent separability profile as difficulty increases from different-verb classes (coarse motion and appearance cues available) through same-verb pairs (shared verb, distinguishable only by direction or object) to pretend-vs-real pairs (separable only by fine contact cues) - Figure 2 (right). In contrast, VideoMAEv2 peaks on different-verb classes but drops sharply on same-verb pairs, with only partial recovery on pretend-vs-real pairs. It also exhibits higher standard deviation within the different-verb category, indicating less consistent separability across classes. Together, these results support the conclusion that V-JEPA representations are more uniform across semantic regimes. This pattern aligns with the hypothesis that joint-embedding predictive objectives capture higher-level semantic structure, whereas masked pixel-reconstruction objectives remain more sensitive to low-level visual distinctiveness. The partial recovery on pretend-vs-real pairs in VideoMAEv2 may reflect exaggerated motion cues in pretending actions that provide distinctive visual signatures despite semantic ambiguity.

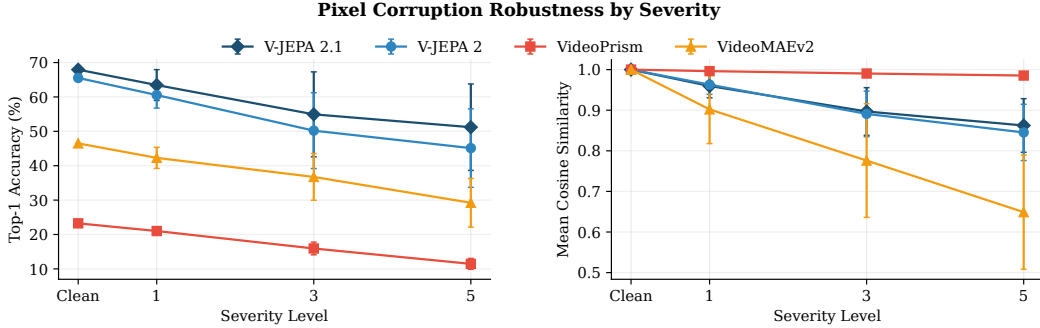


Figure 3: Representational stability as a function of corruption severity, averaged across all six corruption types. **(Left)** Top-1 classification accuracy. **(Right)** cosine similarity.

5 Does latent-prediction optimize for meaning over appearance?

Section 4 established that V-JEPA features exhibit consistent class separability under clean conditions. We now extend our evaluations to six practical corruptions (motion blur, snow, pixelation, impulse noise, brightness, and elastic transform) at three severity levels defined in [17]. Refer to Figure 9 for representative visualizations of the employed input corruptions.

V-JEPA encodes meaning over appearance, yielding systematic robustness under corruption.

Figure 3 (left) presents the aggregate degradation trajectories across all corruption types. V-JEPA 2.1 maintains the highest classification accuracy at every severity level and degrades most gradually, with V-JEPA 2 following closely behind. VideoMAEv2 and VideoPrism exhibit steeper declines, with the ordering among all four models preserved across severity levels. Per-corruption analysis (Appendix C, Figure 10) confirms that V-JEPA 2.1 achieves the highest accuracy retention on five of six corruption types, with the largest margins on corruptions that alter pixel statistics while preserving action semantics, such as impulse noise, snow, and brightness. V-JEPA 2.1 also outperforms V-JEPA 2 on every corruption type, indicating that the architectural and training refinements in the newer release enhance representational quality under distributional shift beyond clean accuracy gains alone. This resilience suggests that the joint-embedding predictive objective learns to discard surface-level visual variation in favor of higher-order temporal and semantic structure. Because V-JEPA’s loss compares learned abstract representations rather than raw pixel values, two inputs that differ only in surface statistics (e.g. added noise or a brightness shift) can map to nearly identical targets, providing no gradient pressure to preserve those statistics. A pixel-reconstruction loss, by contrast, penalises every pixel deviation equally, forcing the encoder to allocate capacity to reproducing textures, lighting, and backgrounds, which becomes a liability when those pixel statistics are corrupted at test time.

Stable representations are not necessarily useful representations. A striking dissociation emerges in the cosine-similarity panel of Figure 3 (right). VideoPrism maintains near-perfect cosine similarity between clean and corrupted features even at the highest severity, yet suffers the lowest accuracy retention among all models. A representation can thus remain geometrically stable while its class-separating structure erodes. V-JEPA exhibits the converse pattern: its cosine similarity under corruption is in fact *lower* than VideoPrism’s (Figure 3, right), yet it retains the highest classification accuracy (Figure 3, left). This dissociation rules out generic invariance as the source of V-JEPA’s robustness and instead points to the selective preservation of information that matters for discrimination. Theoretically, VideoPrism’s contrastive video-text alignment encourages the encoder to map all views of the same concept toward a shared embedding region, producing geometric stability, but this invariance pressure simultaneously compresses the intra-class variation that separates the visually similar categories. V-JEPA does not force invariance; it preserves whatever details help predict missing content, retaining useful distinctions even if the overall representation shifts.

6 Can latent prediction distinguish pretend vs real actions?

We evaluate our foundation models on a pretending action set, comprising 1,992 test videos across 22 fine-grained action classes. Each class describes a simulated or failing version of a physical interaction (e.g., “Pretending to pick something up”), forming a deliberately adversarial probe: the visual appearance, gesture kinematics, and camera viewpoint are nearly identical to their genuine counterparts, yet the defining signal is the absence of physical contact or the failure to complete

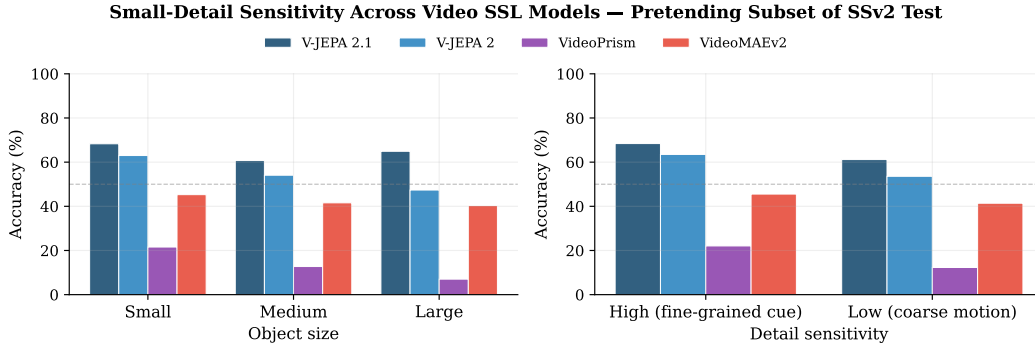


Figure 4: Evaluation on the pretend actions. **(Left)** Actions are categorised based on small, medium and large sizes of the objects involved in the interaction. **(Right)** High sensitivity actions require understanding fine-grained absence-of-contact cues, e.g., empty grasp. Low sensitivity actions are discriminable from coarser object-level motion. Appendix D.1 provides more details on categories.

the interaction. A model that relies on coarse appearance or dominant motion trajectories will be systematically misled. To characterise the nature of each action’s discriminative signal, we partition pretending classes into two groups: *high sensitivity* actions, whose pretend variant is detectable only through fine-grained absence-of-contact cues such as an empty grasp or fluid failing to flow; and *low sensitivity* actions, discriminable from coarser whole-body or object-level motion. We refer to Appendix D.1 for the full categorisation of the actions.

V-JEPA captures fine-grained contact cues despite never reconstructing pixels. A model trained to predict in latent feature space, without ever regenerating individual pixels, might be expected to sacrifice sensitivity to fine-grained visual detail compared to one trained to reconstruct masked spatial content. The results refute this expectation. V-JEPA variants consistently outperform VideoMAEv2 across all object size categories and both detail sensitivity groups (Figure 4), and per-class comparison confirms the advantage spans virtually every individual action class rather than being driven by a few outliers (see Appendix D.3). This pattern suggests that the latent predictive objective distills the spatiotemporal signatures that differentiate real from simulated contact, while pixel reconstruction allocates capacity to surface texture, diluting the contact signal.

The latent-space advantage is stronger where pixel-level training is expected to help the most. The gap between V-JEPA and VideoMAEv2 widens on high sensitivity classes, those requiring detection of subtle absence-of-contact cues such as a fingertip producing no surface reaction or an object undergoing no deformation - Figure 4 (right). VideoMAEv2 derives minimal benefit from the fine-grained contact signal that distinguishes the two sensitivity groups, whereas V-JEPA shows a clear accuracy lift on these classes. This directly contradicts the intuition that reconstructing spatial detail confers an advantage where spatial detail matters most, and instead supports the hypothesis that joint-embedding predictive objectives capture higher-level physical semantics that pixel-level objectives fail to preserve. To predict a masked region’s latent representation, V-JEPA’s encoder must capture abstract state changes, including whether contact occurs and produces a physical effect. Pixel reconstruction spreads capacity across texture and colour details irrelevant to this distinction, diluting the contact signal.

Certain pretend actions are universally unresolvable, exposing a ceiling on visual-only discrimination. Despite the advantage of latent representations, “Pretending or trying and failing to twist something” and “Pretending to take something from somewhere” remain among the hardest classes for all models. In these cases, pretend and real actions look almost identical, with no clear visual cue to distinguish intent. Even the best models make confident mistakes on these classes, concentrating errors on a few inherently hard categories. This pattern suggests a limit of visual information alone, and points to the need for multimodal signals or physical reasoning to resolve such ambiguity (see Appendix D.2, D.4, and D.5).

7 What happens when frames are occluded or missing?

Any video world model deployed in realistic conditions must tolerate missing visual information. Objects disappear behind one another, frames drop, and sensors fail. We probe the occlusion robustness of four video encoders through three complementary paradigms: *Moving Block*, which

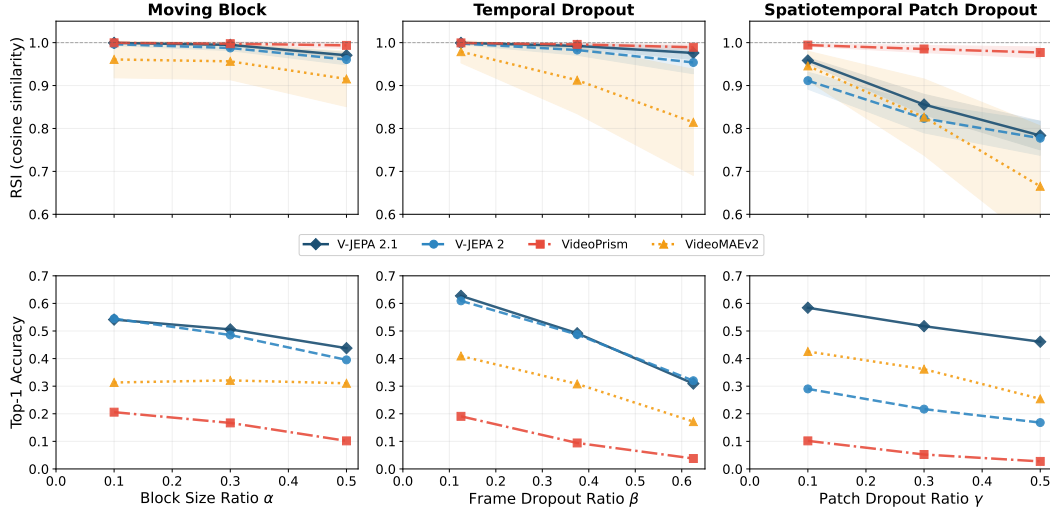


Figure 5: **Top:** Cosine similarity between clean and occluded embeddings as a function of occlusion severity for three paradigms. **Bottom:** Top-1 classification accuracy under the same occlusions.

sweeps a grey square across the spatial extent and isolates spatial robustness; *Temporal Dropout*, which freezes a contiguous block of frames and isolates temporal robustness; and *Spatiotemporal Patch Dropout*, which zeros random 3D cuboids in the video volume and mirrors the masked prediction objective used by V-JEPA. Each paradigm is applied at three severity levels (parameters α, β, γ). Full hyperparameters appear in Appendix E.

Predicting in latent space generalises better to missing input than predicting in pixel space.

Both V-JEPA and VideoMAEv2 are pre-trained with patch masking, yet V-JEPA produces substantially more stable features and retains higher classification accuracy under inference-time occlusion across all three paradigms (Figure 5). VideoMAEv2 degrades the fastest under temporal dropout and patch dropout, exhibiting the steepest cosine-similarity slopes of all encoders. Because these two model families differ primarily in whether the prediction target is a latent representation or the raw pixels, this contrast provides direct evidence that the choice of prediction space, not the masking strategy itself, plays the key role in occlusion robustness.

V-JEPA 2.1 is the most robust encoder for downstream decision making under occlusion. V-JEPA 2.1 leads in probe accuracy under all three occlusion paradigms and sustains the most graceful degradation as severity increases. Among the encoders evaluated, it provides the most dependable feature backbone for a world model that must produce correct decisions from incomplete observations.

Stable representations are not necessarily useful representations (occlusion). The dissociation we observed under corruption in Section 5 is even more starkly manifested in Figure 5. Under spatiotemporal patch dropout at maximum severity, VideoPrism’s embedding shifts by less than two percent in cosine distance while its probe accuracy collapses to near chance. V-JEPA 2.1 sits at the opposite extreme: its representations shift noticeably more, yet it retains the highest probe accuracy across all three paradigms. We also quantify this gap more concretely in per-model Decoupling Index (DI) in Figure 22 in the appendix.

8 Do video models encode the arrow of time?

We probe how much each encoder relies on temporal structure by applying ten perturbation conditions from four families: frame permutation, static video (all frames replaced by a single repeated still), pure noise (Gaussian and uniform), and video reversal. Results for frame permutation, static video, and pure noise are reported in Appendix F; here we focus on the most architecturally discriminating finding.

Only predictive models encode directional semantics. Video reversal retains every frame and every spatial feature while reversing the temporal order, providing a clean test of whether directionality is a meaningful axis in the latent space. All encoders are used *frozen*, so any directional structure observed must have been internalized during pre-training rather than acquired by the attentive probe.

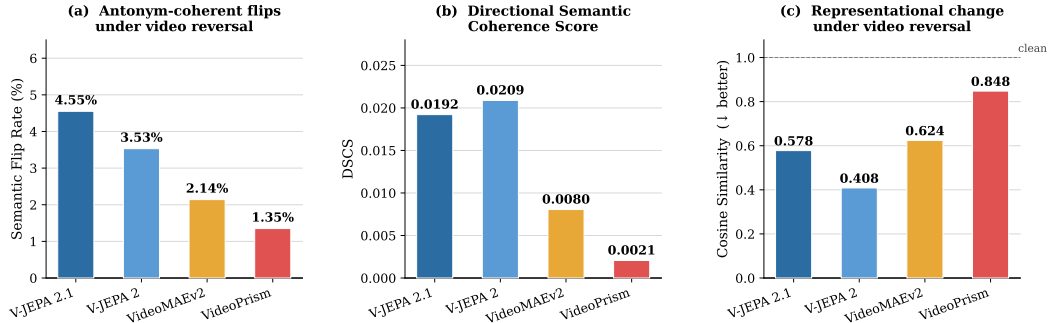


Figure 6: **Video reversal** (a) Semantic Flip Rate (r_{sem}): the fraction of prediction changes under reversal that land on a semantically antonymous class (e.g., *pushing* \rightarrow *pulling*). (b) Directional Semantic Coherence Score (DSCS), which combines the semantic flip rate with the representational distance induced by reversal. (c) Cosine similarity between clean and reversed embeddings.

We quantify this with the Directional Semantic Coherence Score:

$$\text{DSCS} = r_{\text{sem}} \times (1 - \text{cos}_{\text{rev}}),$$

where r_{sem} is the fraction of prediction changes that land on a semantically antonymous class under reversal (e.g., *pushing something from left to right* \rightarrow *pulling something from right to left*) and $(1 - \text{cos}_{\text{rev}})$ is the representational distance induced by reversal. A high DSCS requires both that the representation shifts meaningfully and that the shift is semantically structured.

As shown in Figure 6(a), the V-JEPA models achieve DSCS values several times higher than VideoMAEv2 and VideoPrism. Because the encoder is frozen, this coherent antonym-flipping is a signature of pretraining: temporal direction is internalized as a causal concept, not merely as a source of variation to be averaged out. During pretraining, V-JEPA masks a contiguous block of future patches and predicts their latent representations from earlier context, creating an inherently directional learning signal: the encoder must represent what comes *after* the visible context, not merely what co-occurs with it. The latent space acquires an oriented temporal axis separating “pushing” and “pulling” by direction rather than collapsing them. Contrastive learning suppresses this axis by treating temporal augmentations as positive pairs; pixel reconstruction dilutes it across the pixel-recovery objective. VideoPrism produces the most prediction changes yet the fewest semantically coherent ones, consistent with its stable but unusable embedding behavior observed across corruption and occlusion (Sections 4–7): it detects change but lacks the temporal axis to interpret it.

9 Frozen latent-prediction features vs. task-adapted baselines

Earlier sections showed that V-JEPA leads among frozen encoders under a unified attentive probe. A key question is whether this advantage holds against task-optimised models. Since end-to-end fine-tuning uses label supervision, any remaining edge would suggest that the pretraining objective, not the probe, drives the robustness we observe. We therefore compare V-JEPA 2 (frozen backbone with attentive probe) to VideoMAE and TimeSformer, both fully fine-tuned on SSv2 (Table 2), across corruption robustness, fine-grained pretend action recognition, and occlusion robustness. These evaluations led to the following major insights.

Frozen V-JEPA retains its advantage over fine-tuned baselines for corruption robustness.

Figure 7(a) confirms that V-JEPA 2 leads the models on clean accuracy despite its frozen backbone. We carefully fine-tuned the baselines to get their best performance. As corruption severity increases, the dominance of V-JEPA is preserved, with TimeSformer suffering the steepest accuracy collapse and the largest representational drift, indicating that optimising for clean-condition performance may actively increase brittleness under distributional shift. Finetuning does help in improving the variance profiles of the baselines over V-JEPA, which is expected.

Frozen V-JEPA remains competitive on fine-grained pretend action recognition.

We apply the pretending action evaluation of Section 6 to the models in Table 2, obtaining the results shown in Figure 7(b). V-JEPA 2 closely matches the fine-tuned VideoMAE on top-1 accuracy while substantially outperforming TimeSformer, despite relying solely on an attentive probe. In these results, the gap of V-JEPA 2 to a fully optimised model narrows on the subset demanding physical detail

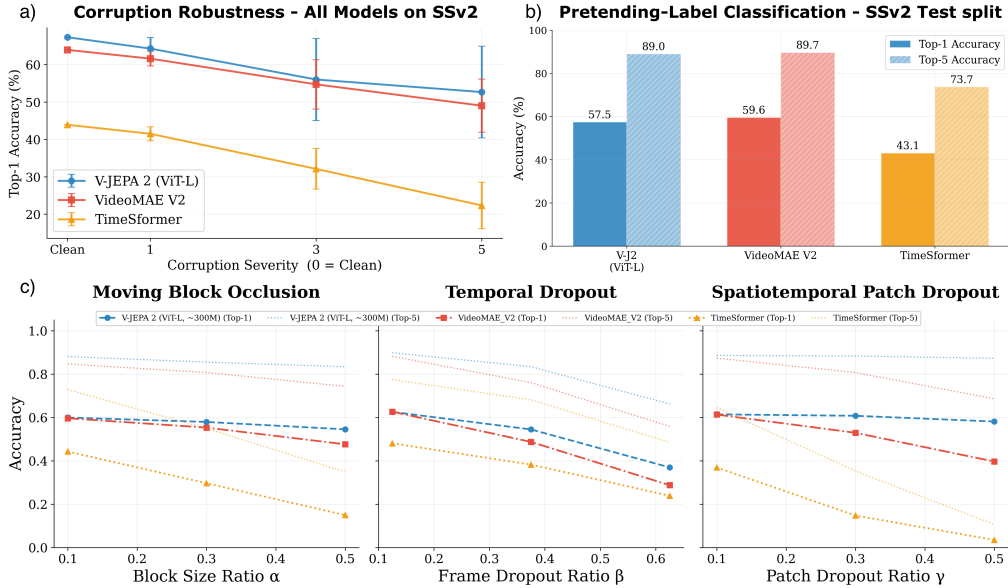


Figure 7: **(a)** Corruption robustness: Representational stability measured by classification accuracy. **(b)** Top-1 and Top-5 accuracy on SSv2 pretending action subset. **(c)** Top-1 and Top-5 accuracy of the models under three occlusion conditions with varying intensity.

discrimination, which is consistent with the finding in Section 6 that latent predictive representations retain fine-grained contact cues in the frozen state.

Frozen V-JEPA representations are more occlusion-robust than fine-tuned backbones. We repeat the three occlusion paradigms from Section 7 on the same models in Figure 7(c). V-JEPA 2 leads in both Top-1 accuracy and representational stability across all three paradigms and severity levels. The collapse of the fine-tuned models under the highest occlusion settings, despite being trained directly on the evaluation distribution, further supports the view that task-specific adaptation optimises for clean-condition performance at the cost of tolerance to missing information.

10 Conclusion

We presented an extensive evaluation laying down empirical foundations for world modeling through self-supervised video representation learning. Our evaluation shows that across a multitude of robustness axes, latent prediction emerges as the video pretraining paradigm that produces a uniformly strong representation. The same models that resist pixel corruption also tolerate occlusion, better distinguish pretend actions from their real counterparts, and respond coherently to temporal reversal. These behaviours are not independent strengths but related outcomes of how the objective shapes the representation. VideoPrism shows the opposite case: a representation can remain geometrically stable while losing the structure that classification relies on, which means cosine similarity alone is an insufficient measure of representational quality. The advantage of latent prediction even holds against task adaptation, as a frozen V-JEPA 2 backbone with a lightweight attentive probe surpasses fully fine-tuned models on corruption and occlusion. We read this as evidence that the pretraining objective, more than scale or label supervision, determines whether a video representation behaves as a world model rather than a clean-benchmark classifier. Our work also implicates that progress in video foundation models cannot be tracked by a single accuracy score, and a multi-axes evaluation is necessary to capture the structural differences that become important beyond curated test sets.

Limitations. While our work provides a thorough robustness evaluation of video world models, the analysis could still be extended along other directions. For instance, we do not cover the cases of adversarial robustness and intentional model manipulation. Our results provide strong motivation and ground work for such exploration by uncovering intriguing insights into the potential of latent prediction paradigm for world modeling. Hence, future work portends further efforts in extending the analyses to also include adversarial axes.

Acknowledgements

Naveed Akhtar is a recipient of the Australian Research Council Discovery Early Career Researcher Award (project # DE230101058) funded by the Australian Government. Ali Alrasheed is also supported by project # DE230101058. This research was also supported by The University of Melbourne’s Research Computing Services and the Petascale Campus Initiative.

References

- [1] Niket Agarwal, Arslan Ali, Maciej Bala, Yogesh Balaji, Erik Barker, Tiffany Cai, Prithvijit Chattopadhyay, Yongxin Chen, Yin Cui, Yifan Ding, et al. Cosmos world foundation model platform for physical ai. *arXiv preprint arXiv:2501.03575*, 2025.
- [2] Mahmoud Assran, Quentin Duval, Ishan Misra, Piotr Bojanowski, Pascal Vincent, Michael Rabbat, Yann LeCun, and Nicolas Ballas. Self-supervised learning from images with a joint-embedding predictive architecture. In *Proceedings of the IEEE/CVF conference on computer vision and pattern recognition*, pages 15619–15629, 2023.
- [3] Mido Assran, Adrien Bardes, David Fan, Quentin Garrido, Russell Howes, Matthew Muckley, Ammar Rizvi, Claire Roberts, Koustuv Sinha, Artem Zholus, et al. V-jepa 2: Self-supervised video models enable understanding, prediction and planning. *arXiv preprint arXiv:2506.09985*, 2025.
- [4] Adrien Bardes, Quentin Garrido, Jean Ponce, Xinlei Chen, Michael Rabbat, Yann LeCun, Mido Assran, and Nicolas Ballas. V-jepa: Latent video prediction for visual representation learning. 2023.
- [5] Gedas Bertasius, Heng Wang, and Lorenzo Torresani. Is space-time attention all you need for video understanding? In *Icml*, volume 2, page 4, 2021.
- [6] Mathilde Caron, Hugo Touvron, Ishan Misra, Hervé Jégou, Julien Mairal, Piotr Bojanowski, and Armand Joulin. Emerging properties in self-supervised vision transformers. In *Proceedings of the IEEE/CVF international conference on computer vision*, pages 9650–9660, 2021.
- [7] Ting Chen, Simon Kornblith, Mohammad Norouzi, and Geoffrey Hinton. A simple framework for contrastive learning of visual representations. In *International conference on machine learning*, pages 1597–1607. PmlR, 2020.
- [8] Quentin Garrido, Nicolas Ballas, Mahmoud Assran, Adrien Bardes, Laurent Najman, Michael Rabbat, Emmanuel Dupoux, and Yann LeCun. Intuitive physics understanding emerges from self-supervised pretraining on natural videos. *arXiv preprint arXiv:2502.11831*, 2025.
- [9] Raghav Goyal, Samira Ebrahimi Kahou, Vincent Michalski, Joanna Materzynska, Susanne Westphal, Heuna Kim, Valentin Haebel, Ingo Fruend, Peter Yianilos, Moritz Mueller-Freitag, et al. The "something something" video database for learning and evaluating visual common sense. In *Proceedings of the IEEE international conference on computer vision*, pages 5842–5850, 2017.
- [10] Jean-Bastien Grill, Florian Strub, Florent Altché, Corentin Tallec, Pierre Richemond, Elena Buchatskaya, Carl Doersch, Bernardo Avila Pires, Zhaohan Guo, Mohammad Gheshlaghi Azar, et al. Bootstrap your own latent—a new approach to self-supervised learning. *Advances in neural information processing systems*, 33:21271–21284, 2020.
- [11] David Ha and Jürgen Schmidhuber. World models. *arXiv preprint arXiv:1803.10122*, 2(3):440, 2018.
- [12] Danijar Hafner, Timothy Lillicrap, Jimmy Ba, and Mohammad Norouzi. Dream to control: Learning behaviors by latent imagination. *arXiv preprint arXiv:1912.01603*, 2019.
- [13] Danijar Hafner, Timothy Lillicrap, Mohammad Norouzi, and Jimmy Ba. Mastering atari with discrete world models. *arXiv preprint arXiv:2010.02193*, 2020.
- [14] Danijar Hafner, Jurgis Pasukonis, Jimmy Ba, and Timothy Lillicrap. Mastering diverse domains through world models. *arXiv preprint arXiv:2301.04104*, 2023.

- [15] Danijar Hafner, Wilson Yan, and Timothy Lillicrap. Training agents inside of scalable world models. *arXiv preprint arXiv:2509.24527*, 2025.
- [16] Kaiming He, Xinlei Chen, Saining Xie, Yanghao Li, Piotr Dollár, and Ross Girshick. Masked autoencoders are scalable vision learners. In *Proceedings of the IEEE/CVF conference on computer vision and pattern recognition*, pages 16000–16009, 2022.
- [17] Dan Hendrycks and Thomas Dietterich. Benchmarking neural network robustness to common corruptions and perturbations. *arXiv preprint arXiv:1903.12261*, 2019.
- [18] De-An Huang, Vignesh Ramanathan, Dhruv Mahajan, Lorenzo Torresani, Manohar Paluri, Li Fei-Fei, and Juan Carlos Niebles. What makes a video a video: Analyzing temporal information in video understanding models and datasets. In *Proceedings of the IEEE Conference on Computer Vision and Pattern Recognition*, pages 7366–7375, 2018.
- [19] Sonia Joseph, Quentin Garrido, Randall Balestriero, Matthew Kowal, Thomas Fel, Shahab Bakhtiari, Blake Richards, and Mike Rabbat. Interpreting physics in video world models. *arXiv preprint arXiv:2602.07050*, 2026.
- [20] Yann LeCun et al. A path towards autonomous machine intelligence version 0.9. 2, 2022-06-27. *Open Review*, 62(1):1–62, 2022.
- [21] Lorenzo Mur-Labadia, Matthew Muckley, Amir Bar, Mido Assran, Koustuv Sinha, Mike Rabbat, Yann LeCun, Nicolas Ballas, and Adrien Bardes. V-jepa 2.1: Unlocking dense features in video self-supervised learning. *arXiv preprint arXiv:2603.14482*, 2026.
- [22] Muhammad Muzammal Naseer, Kanchana Ranasinghe, Salman H Khan, Munawar Hayat, Fahad Shahbaz Khan, and Ming-Hsuan Yang. Intriguing properties of vision transformers. *Advances in Neural Information Processing Systems*, 34:23296–23308, 2021.
- [23] Jack Parker-Holder, Philip Ball, Jake Bruce, Vibhavari Dasagi, Kristian Holsheimer, Christos Kaplanis, Alexandre Moufarek, Guy Scully, Jeremy Shar, Jimmy Shi, et al. Genie 2: A large-scale foundation world model. URL: <https://deepmind.google/discover/blog/genie-2-a-large-scale-foundation-world-model>, 2, 2024.
- [24] Sayak Paul and Pin-Yu Chen. Vision transformers are robust learners. In *Proceedings of the AAAI conference on Artificial Intelligence*, volume 36, pages 2071–2081, 2022.
- [25] Laura Sevilla-Lara, Shengxin Zha, Zhicheng Yan, Vedanuj Goswami, Matt Feiszli, and Lorenzo Torresani. Only time can tell: Discovering temporal data for temporal modeling. In *Proceedings of the IEEE/CVF winter conference on applications of computer vision*, pages 535–544, 2021.
- [26] Zhan Tong, Yibing Song, Jue Wang, and Limin Wang. Videomae: Masked autoencoders are data-efficient learners for self-supervised video pre-training. *Advances in neural information processing systems*, 35:10078–10093, 2022.
- [27] Limin Wang, Bingkun Huang, Zhiyu Zhao, Zhan Tong, Yinan He, Yi Wang, Yali Wang, and Yu Qiao. Videomae v2: Scaling video masked autoencoders with dual masking. In *Proceedings of the IEEE/CVF conference on computer vision and pattern recognition*, pages 14549–14560, 2023.
- [28] Sukmin Yun, Jaehyung Kim, Dongyoon Han, Hwanjun Song, Jung-Woo Ha, and Jinwoo Shin. Time is matter: Temporal self-supervision for video transformers. *arXiv preprint arXiv:2207.09067*, 2022.
- [29] Long Zhao, Nitesh B Gundavarapu, Liangzhe Yuan, Hao Zhou, Shen Yan, Jennifer J Sun, Luke Friedman, Rui Qian, Tobias Weyand, Yue Zhao, et al. Videoprism: A foundational visual encoder for video understanding. *arXiv preprint arXiv:2402.13217*, 2024.
- [30] Gaoyue Zhou, Hengkai Pan, Yann LeCun, and Lerrel Pinto. Dino-wm: World models on pre-trained visual features enable zero-shot planning. *arXiv preprint arXiv:2411.04983*, 2024.

This appendix provides extended experimental details and additional analyses for each section of the main paper. We begin with global methodological context in Appendix A (encoder selection criteria and attentive-probe training protocol). The remaining sections mirror the order of the five main-paper evaluation axes: Feature Discriminability (Appendix B), Corruption Robustness (Appendix C), Fine-Grained Action Discrimination (Appendix D), Occlusion Robustness (Appendix E), and Temporal Robustness (Appendix F). Details of the fine-tuned and supervised baselines used in Section 9 are provided in Appendix A.2.

A Model comparison considerations

Table 3 summarises the key attributes of each encoder evaluated in this study. The four models were selected to span the three dominant self-supervised video paradigms at matched ViT-L capacity (~ 300 M parameters), so that observed differences are most naturally attributed to the pretraining objective. We acknowledge that pretraining data composition, data scale, and training schedule are not fully controlled across models—full ablation of these factors would require retraining each model from scratch under identical data and compute budgets, which is beyond our scope. Nevertheless, the consistent behavioural clustering we observe—both V-JEPA variants forming one group and both non-JEPA models forming another across all five evaluation axes—is difficult to attribute to data alone, particularly because V-JEPA 2 and VideoPrism both train on large-scale heterogeneous video corpora yet diverge sharply in every robustness metric.

Table 3: Detailed comparison of the four evaluated encoders. All models use a ViT-Large backbone.

Model	Params	Pretraining Data	Objective	Source
V-JEPA 2.1	~ 300 M	Internet video (> 1 M hrs)	Latent prediction	Meta
V-JEPA 2	~ 300 M	Internet video (> 1 M hrs)	Latent prediction	Meta
VideoPrism	~ 300 M	Video + video-text pairs (36M clips)	Contrastive + masked pred.	Google
VideoMAEv2	~ 300 M	UnlabeledHybrid (mix of public sets)	Pixel reconstruction	Open-source

A.1 Attentive probe training protocol

For each encoder, we invested approximately 100 A100 GPU-hours in attentive probe training, exploring multiple configurations (varying depth, number of heads, MLP ratio, and learning rate). The best-performing probe configuration was selected for each model based on clean validation accuracy on Something-Something v2. This protocol ensures that each encoder is evaluated under its most favourable probe setting, so that the relative ordering across models reflects genuine differences in frozen representation quality rather than artefacts of probe mismatch. The total probe training budget across all four models was approximately 400 A100 GPU-hours; together with the perturbation evaluation runs, the full experimental pipeline consumed approximately 1,000 GPU-hours.

A.2 Fine-tuned model checkpoints

For the training-regime comparison in Section 9, we rely exclusively on publicly released checkpoints that have been adapted to Something-Something v2, in order to avoid confounds introduced by our own fine-tuning hyperparameters. Because no single provider releases matched ViT-L fine-tuned checkpoints across all three training regimes on SSv2, the backbones differ slightly in capacity and input configuration; we describe each below.

- **V-JEPA 2 (frozen backbone, attentive-probe only).** We use the ViT-L/16 V-JEPA 2 encoder released by Meta, with 64 frames at 256×256 resolution.
- **VideoMAE (end-to-end fine-tuned).** We use the `videomae-base-finetuned-ssv2` checkpoint released by MCG-NJU, which is pre-trained for 2400 epochs with masked pixel reconstruction and then end-to-end fine-tuned on SSv2 with full supervision. This is the only VideoMAE SSv2 checkpoint publicly available at the time of writing; it is a ViT-B/16 backbone consuming 16 frames at 224×224 , and reaches 70.6% top-1 and 92.6% top-5 on the SSv2 test set.

Table 4: The 30 SSv2 action classes used in the encoder discriminability analysis, grouped by semantic category and ordered by increasing semantic difficulty (different-verb < same-verb < pretend-vs-real).

Semantic Category	Action Class
<i>Different Verbs</i>	Burying something in something
	Closing something
	Folding something
	Hitting something with something
	Plugging something into something
	Removing something, revealing something behind
	Spinning something so it continues spinning
	Stacking number of something
	Tearing something into two pieces
	Trying but failing to attach something to something
<i>Same Verb</i>	Moving away from something with your camera
	Moving part of something
	Poking a hole into something soft
	Poking a stack of something so the stack collapses
	Pulling something from behind of something
	Pulling something from left to right
	Pushing something from left to right
	Pushing something from right to left
	Putting something and something on the table
	Putting something behind something
<i>Pretend vs Real</i>	Poking a hole into some substance
	Pretending to poke something
	Pouring something into something
	Pretending to pour something out of something
	Putting number of something onto something
	Pretending to put something behind something
	Throwing something
	Pretending to throw something
	Turning something upside down
	Pretending to turn something upside down

- **TimeSformer (fully supervised).** We use the high-frame-count TimeSformer variant trained end-to-end on SSv2 from ImageNet-21k initialisation, consuming 64 frames at 224×224 with divided space-time attention. No self-supervised stage is involved; the backbone is optimised jointly with the classification head under label supervision.

All three models are evaluated on the same perturbation suite used for the frozen encoders (Sections 5, 6, and 7), with perturbations applied to the pre-processed input at the resolution and frame count native to each checkpoint. Because the VideoMAE checkpoint is ViT-B rather than ViT-L, the comparison in Section 9 should be interpreted as a capability-level rather than capacity-matched comparison: the frozen ViT-L V-JEPA 2 backbone nonetheless exceeds the fully fine-tuned baselines on corruption and occlusion robustness, which strengthens rather than weakens the conclusion.

B Feature discriminability: supplementary analysis

B.1 Action class list

Details are shown in Table 4

B.2 Architecture attribution

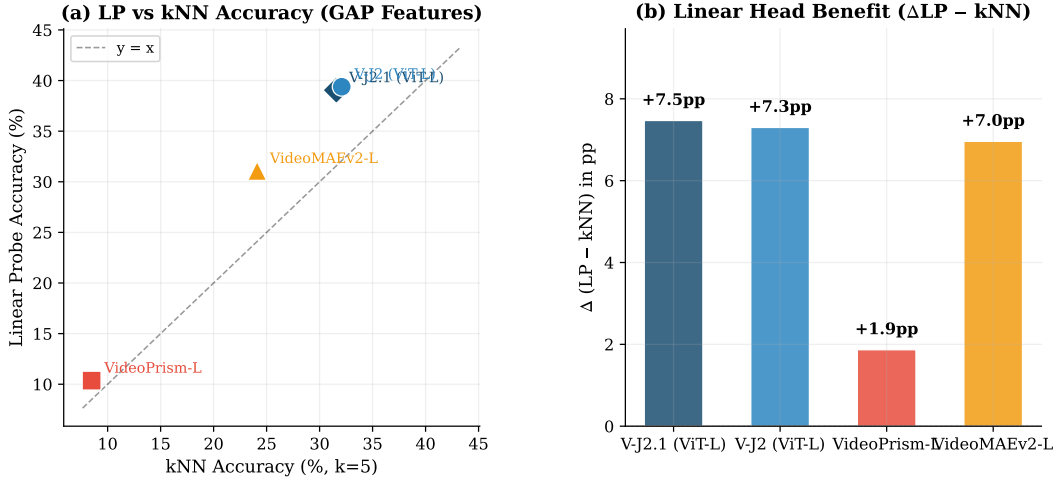


Figure 8: Architecture attribution via GAP features. **(a)** Linear probe vs kNN accuracy; points above the diagonal indicate a linear head adds value beyond geometric proximity. **(b)** The gap $\Delta(LP - kNN)$ is largest for V-JEPA models, suggesting their representations encode direction-dependent semantic structure exploitable by a linear classifier.

C Corruption robustness: supplementary analysis

C.1 Visual examples of corruptions

Figure 9 illustrates the six corruption types at all three severity levels applied to a sample video frame, providing visual reference for the perturbation intensities used throughout the experiment.

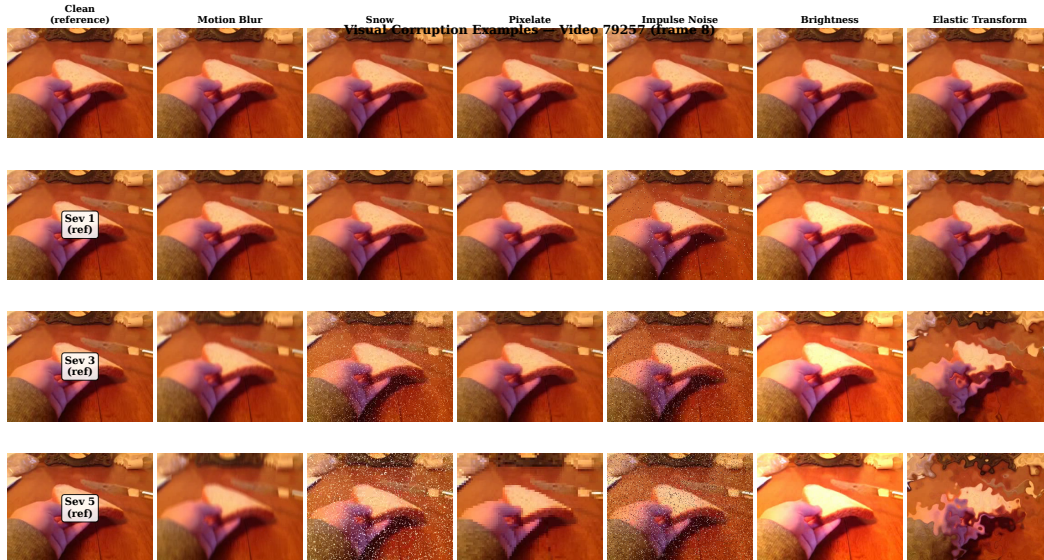


Figure 9: Visual examples of the six corruption types applied to a single SSv2 video frame at severities 1, 3, and 5. Columns correspond to corruption types and rows to increasing severity, illustrating the progressive degradation of visual content.

C.2 Per-corruption accuracy retention at maximum severity

Figure 10 reports accuracy retention at severity 5 as a percentage of each model’s clean baseline. V-JEPA 2.1 leads on five of six corruption types. Elastic transform is the universal outlier, reducing all models to near-zero or single-digit retention, with VideoMAEv2 exhibiting the most severe collapse. Brightness and motion blur are the least disruptive corruptions for both V-JEPA variants, consistent with the expectation that photometric perturbations preserving temporal structure are well handled by joint-embedding objectives.

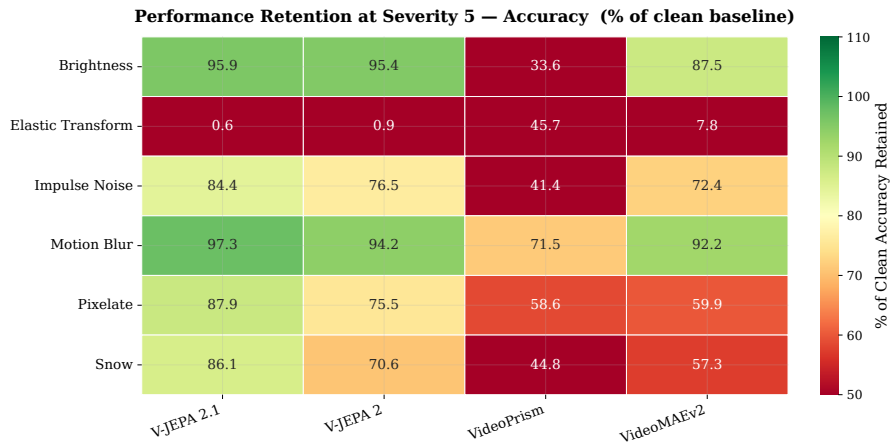


Figure 10: Per-corruption accuracy retention at severity 5 (% of clean baseline retained). V-JEPA 2.1 leads on five of six corruption types, while elastic transform is universally the most damaging.

C.3 Cosine similarity retention

Figure 11 shows cosine similarity retention at severity 5. VideoPrism retains near-perfect similarity across all corruptions, yet this stability does not prevent its classification accuracy from declining sharply (Figure 10). VideoMAEv2 shows the largest representational drift under elastic transform, confirming that pixel-reconstruction encoders are particularly sensitive to geometric distortions at the feature level.

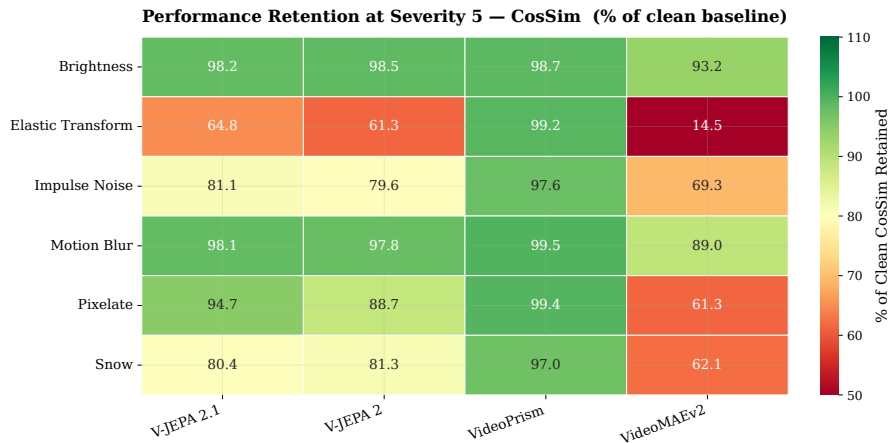


Figure 11: Per-corruption cosine similarity retention at severity 5 (% of clean baseline). VideoPrism maintains near-perfect representational stability despite declining accuracy, while VideoMAEv2 exhibits severe feature drift under elastic transform.

C.4 Per-model degradation profiles

Figure 12 decomposes the aggregate severity curves into per-corruption trajectories for each model. For V-JEPA 2.1 and V-JEPA 2, most corruptions cluster in a narrow band of gradual decline, with elastic transform as a clear outlier dropping steeply. VideoMAEv2 shows a wider spread among corruption types, reflecting greater sensitivity to the nature of the perturbation. VideoPrism exhibits uniformly low absolute accuracy across all corruptions, making relative differences less pronounced.

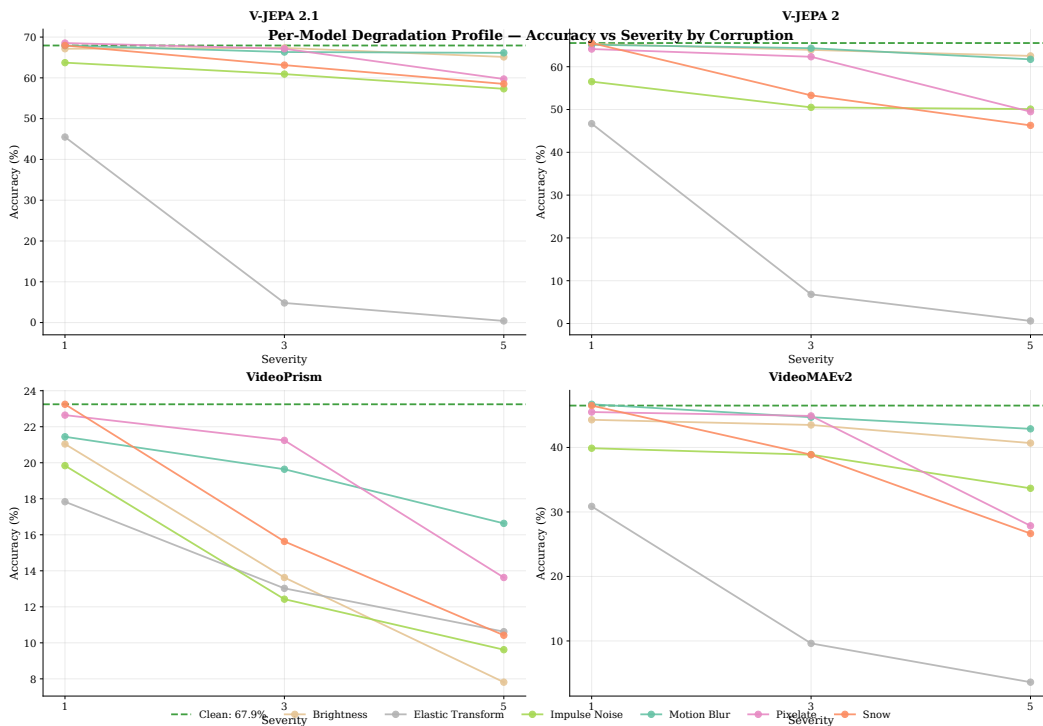


Figure 12: Per-model accuracy as a function of severity for each corruption type. Most corruptions cluster together for V-JEPA variants, while elastic transform is a clear outlier for all models except VideoPrism.

C.5 Degradation slopes

Figure 13 reports the accuracy degradation slope for each model and corruption type, measured in percentage points per severity level. Elastic transform produces the steepest slopes for V-JEPA 2, V-JEPA 2.1, and VideoMAEv2, while brightness is the steepest for VideoPrism. V-JEPA 2.1 exhibits shallower slopes than V-JEPA 2 on every corruption type, quantifying the robustness improvement of the newer release.

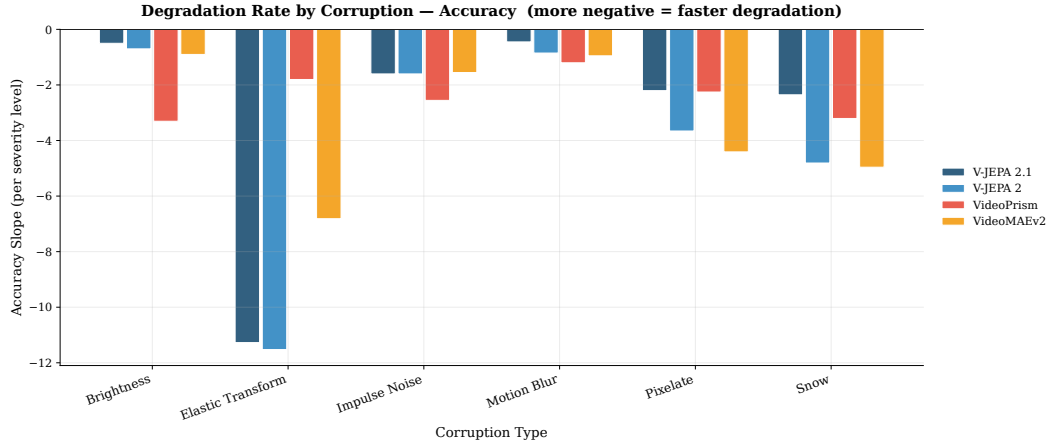


Figure 13: Accuracy degradation slope per corruption type (pp per severity level; more negative indicates faster decline). V-JEPA 2.1 consistently shows the shallowest degradation.

D Fine-grained action discrimination: supplementary analysis

D.1 Class categorisation

We partition the 22 pretending action classes along two dimensions using a verb-based heuristic applied to the SSv2 label text. **Object size** is assigned based on the primary verb: actions involving manipulation of small items (e.g., *pick*, *poke*, *squeeze*, *pour*, *wipe*) are labelled *small*; actions involving state changes to moderate-scale objects (e.g., *twist*, *tear*, *open*, *close*, *take*) are labelled *medium*; and actions involving large spatial displacement (e.g., *throw*) are labelled *large*. **Detail sensitivity** captures whether the pretend variant is distinguishable only through fine-grained contact cues (*high*) or through coarser whole-body or object-level motion (*low*). The complete mapping is given in Table 5.

Table 5: Categorisation of the 22 pretend action classes by object size and detail sensitivity.

Action Class	Object Size	Detail Sensitivity
P. or failing to wipe something off of something	small	high
P. to pick something up	small	high
P. to poke something	small	high
P. to pour something out of something. . .	small	high
P. to put something behind something	small	high
P. to put something into something	small	high
P. to put something next to something	small	high
P. to put something on a surface	small	high
P. to put something onto something	small	high
P. to put something underneath something	small	high
P. to spread air onto something	small	high
P. to sprinkle air onto something	small	high
P. to squeeze something	small	high
P. to scoop something up with something	small	low
P. or trying and failing to twist something	medium	low
P. to be tearing something that is not tearable	medium	low
P. to close something without actually closing it	medium	low
P. to open something without actually opening it	medium	low
P. to take something from somewhere	medium	low
P. to take something out of something	medium	low
P. to turn something upside down	medium	low
P. to throw something	large	low

D.2 Hardest pretend actions

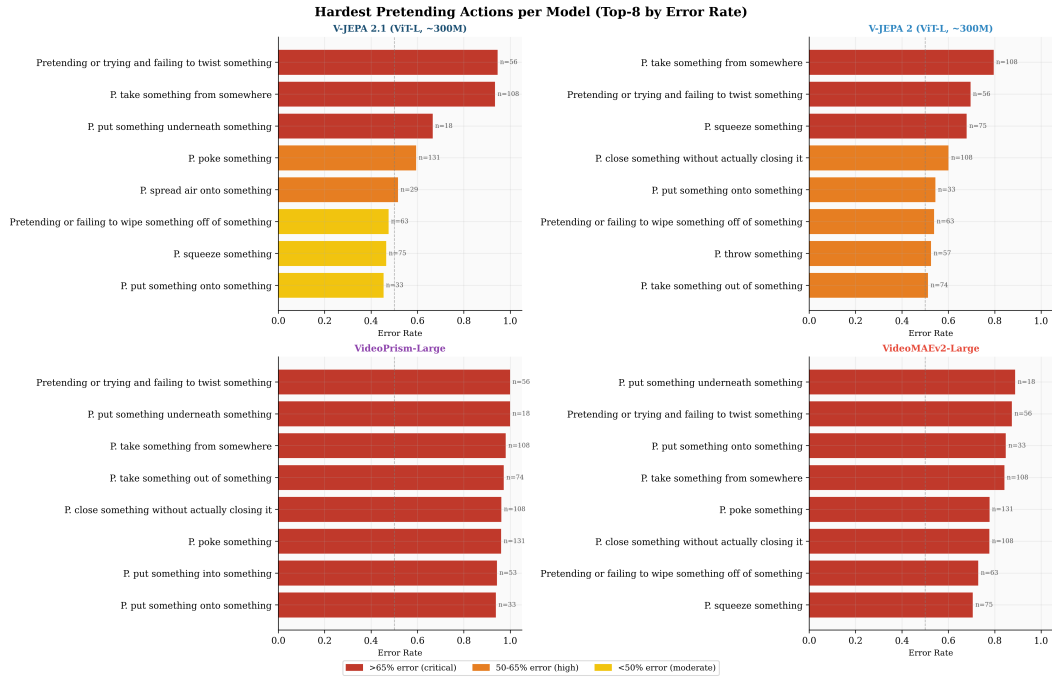


Figure 14: Top eight hardest pretend action classes per model by error rate, colour-coded by severity (red: critical, orange: high, yellow: moderate).

Figure 14 reports the top eight hardest pretending action classes per model, ranked by error rate. “Pretending or trying and failing to twist something” and “Pretending to take something from somewhere” appear among the top three for all four models, confirming that these failures are architecture-agnostic and arise from inherent kinematic ambiguity in the action classes themselves.

D.3 Per-class accuracy delta

Figure 15 presents the per-class accuracy difference between the appearance-focused model (VideoMAEv2-Large) and each latent-space variant, with bars colour-coded by object size. Negative values indicate that the latent model outperforms. The latent-space approach dominates across virtually all action classes and object size strata, with the appearance-focused model winning none of the small-object classes against either V-JEPA variant and at most two medium-object classes against V-JEPA 2.1.



Figure 15: Per-class accuracy delta (VideoMAEv2-Large minus V-JEPA variant; positive values indicate VideoMAEv2 wins), colour-coded by object size.

D.4 High-stakes error analysis

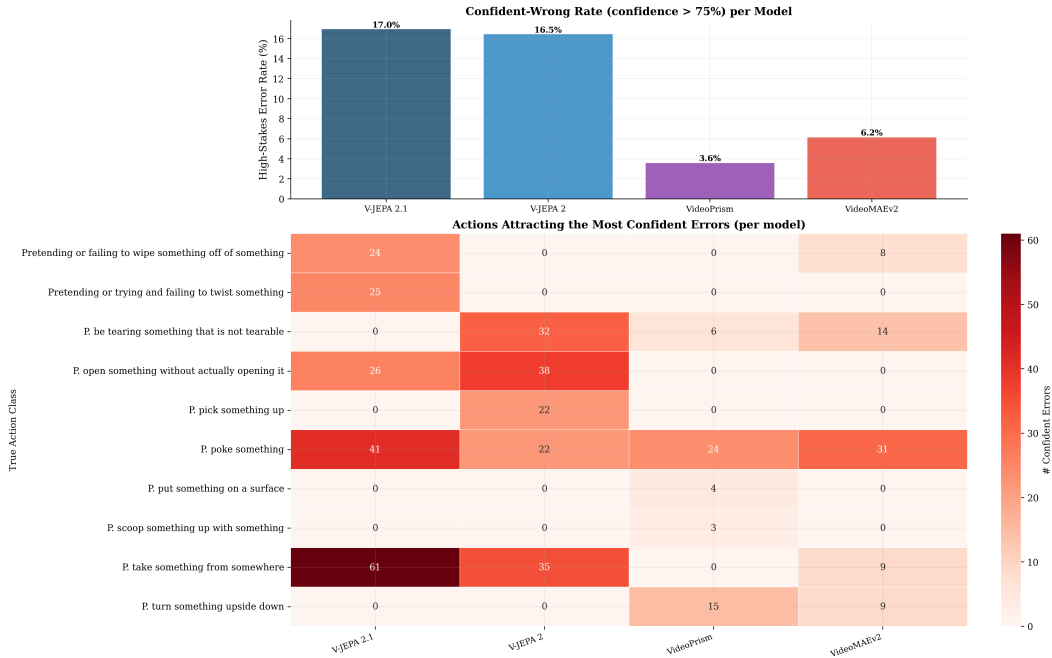


Figure 16: Top: confident-wrong rate (confidence > 75%, prediction incorrect) per model. Bottom: heatmap of high-stakes errors across action classes, showing concentration on universally hard categories.

Figure 16 examines confident misclassifications (predictions with confidence exceeding 75% that are incorrect). The stronger latent-space models exhibit higher overall high-stakes error rates than the appearance-focused or vision-language models, yet the bottom panel reveals that these errors concentrate on a small number of universally hard classes rather than being distributed across the label space. This indicates structured failure at the boundary of visual ambiguity rather than a systemic calibration deficit.

D.5 Calibration analysis

Figure 17 plots per-class accuracy against mean prediction confidence, with bubble size proportional to sample count and colour indicating detail sensitivity. The shaded region marks overconfident classes (mean confidence above 70%, accuracy below 40%). The V-JEPA variants each contain two classes in this region, both corresponding to the architecture-agnostic failure modes identified above, while the appearance-focused and vision-language models contain none. This confirms that the elevated high-stakes error rate of stronger models is a localised phenomenon tied to inherent class ambiguity, not a general calibration failure.

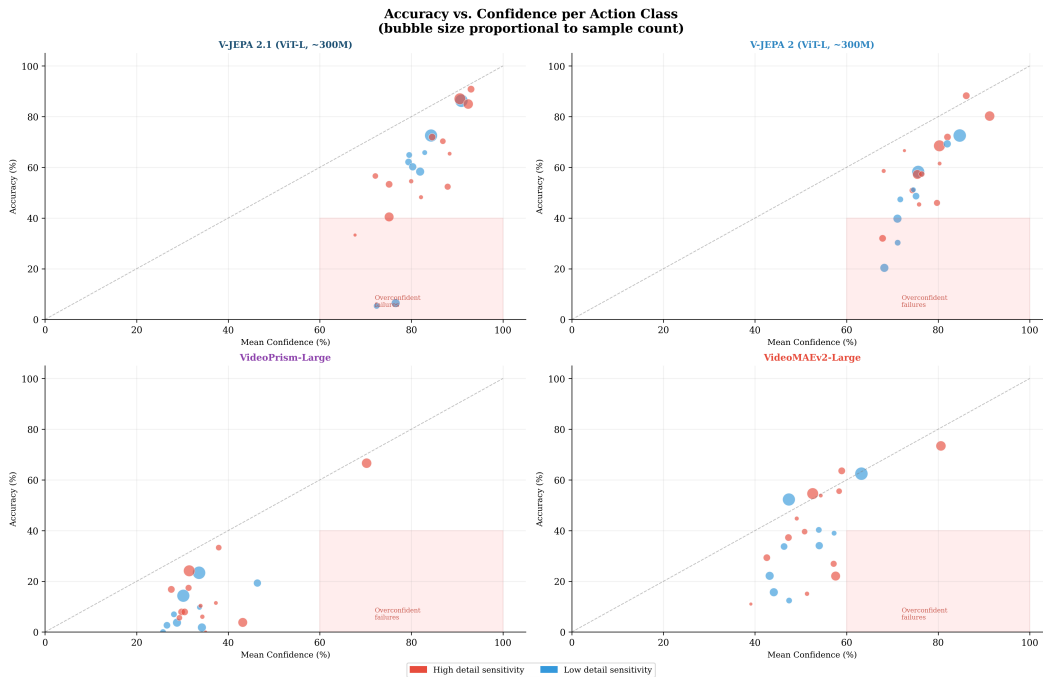


Figure 17: Per-class accuracy versus mean confidence (bubble size \propto sample count). Shaded region: overconfident classes (confidence > 70%, accuracy < 40%). V-JEPA variants each have two overconfident classes; VideoMAEv2 and VideoPrism have none.

E Occlusion robustness: supplementary analysis

E.1 Experimental hyperparameters

Component	Setting
Dataset	Something-Something v2, test split
Number of clips	1,740
Number of classes	174
Frames per clip	16, uniformly sampled
Random seed	42
Encoders evaluated	V-JEPA 2.1 (ViT-L, ~300M), V-JEPA 2 (ViT-L, ~300M), VideoPrism-Large, VideoMAEv2-Large
Moving Block ratio α	$\{0.10, 0.30, 0.50\}$ of $\min(H, W)$
Temporal Dropout ratio β	$\{0.125, 0.375, 0.625\}$ of T
Patch Dropout ratio γ	$\{0.10, 0.30, 0.50\}$ of 3D cuboids
Patch Dropout cuboid size	$(\tau=2, p=16, p=16)$
Attentive probe depth	2
Attentive probe heads	8
Attentive probe MLP ratio	2.0
kNN probe neighbours	$k = 5$, cosine metric, standardised features

Table 6: Hyperparameters for the occlusion robustness benchmark. All severities are evaluated on the same set of clean clips so that pairs are matched at the clip level before computing RSI, CCR, and probe accuracy.

E.2 Metric definitions

For paired clean and occluded embeddings $f_i^c, f_i^o \in \mathbb{R}^D$ over N clips:

$$\begin{aligned} \text{RSI} &= \frac{1}{N} \sum_{i=1}^N \frac{\langle f_i^c, f_i^o \rangle}{\|f_i^c\| \|f_i^o\|}, \\ \text{CCR} &= \frac{1}{N} \sum_{i=1}^N \mathbf{1}[\hat{y}_{\text{kNN}}(f_i^c) = \hat{y}_{\text{kNN}}(f_i^o)], \\ \text{AUC(RSI)} &= \int_0^{s_{\max}} \text{RSI}(s) ds. \end{aligned}$$

The kNN classifier is fit on clean features and reused at evaluation, so CCR measures whether the same clip is routed to the same neighbourhood.

E.3 Visualisations of each occlusion paradigm

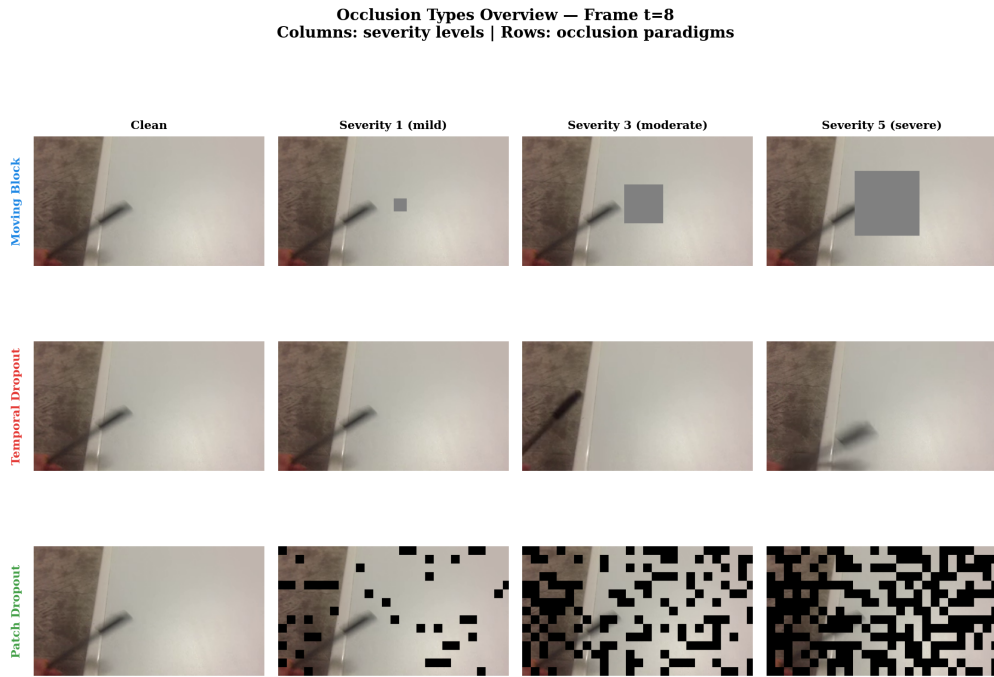


Figure 18: Overview of the three occlusion paradigms at increasing severity on a single representative clip.

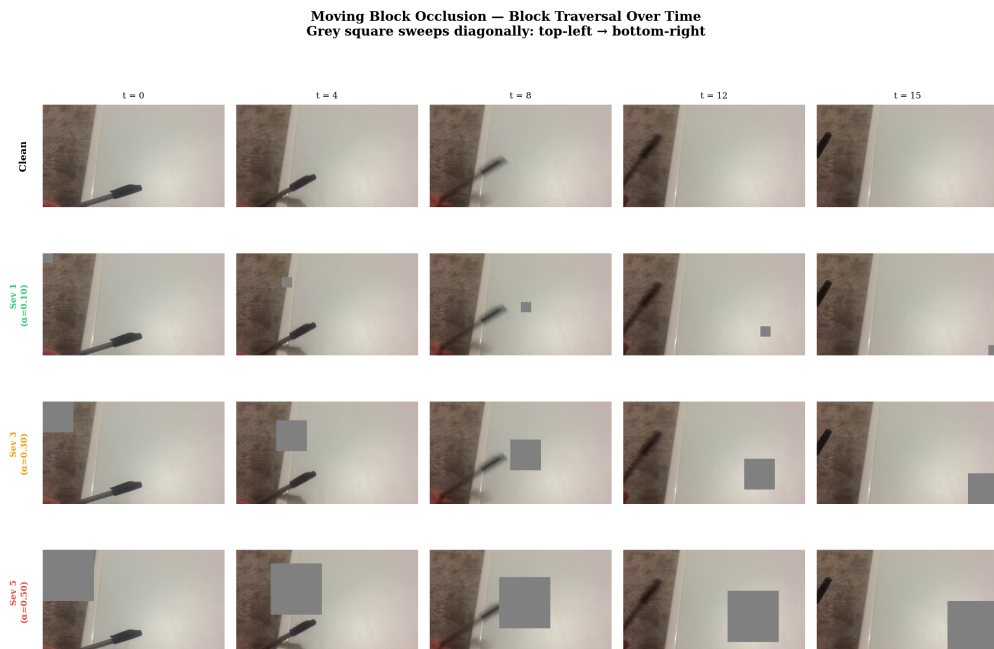


Figure 19: Moving Block at five timestamps. The grey square traverses the frame diagonally so that any single moment occludes a different region. The block side is $\alpha \cdot \min(H, W)$.

Temporal Dropout – Frame Freeze Effect
 Red border = frozen frames (last visible frame repeated). Columns chosen to bracket the freeze onset/offset.

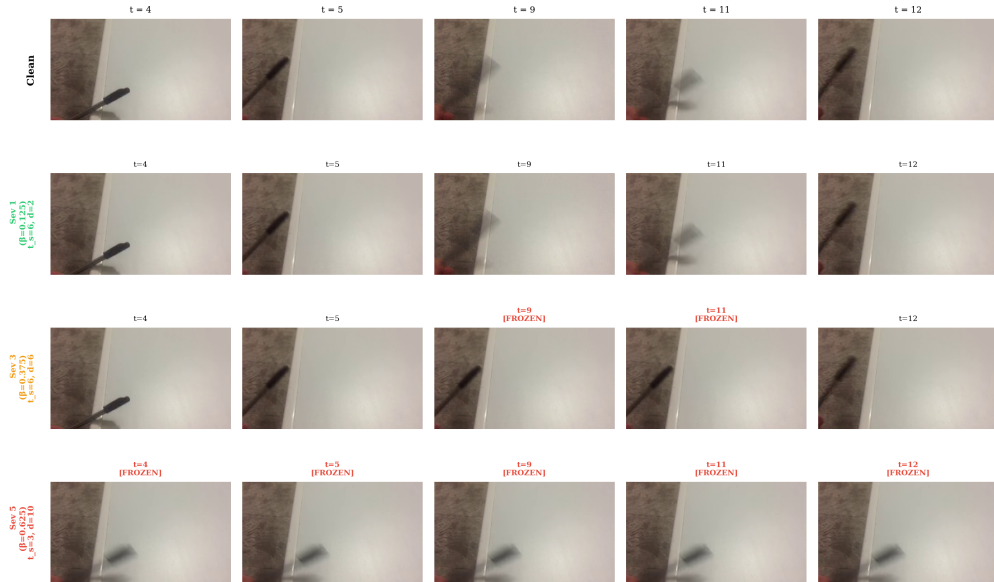


Figure 20: Temporal Dropout. A contiguous block of $\lfloor \beta T \rfloor$ frames is replaced by repeating the last visible frame. We show frames just before the gap, at the onset, mid gap, and at recovery.

E.4 Additional analyses

Severity slopes. Linear regression of RSI on the severity parameter gives a per model degradation rate. Steeper negative slopes indicate faster collapse.

Model	Moving Block	Temporal Dropout	Patch Dropout
V-JEPA 2.1	-0.072	-0.047	-0.437
V-JEPA 2	-0.089	-0.088	-0.335
VideoPrism	-0.015	-0.020	-0.043
VideoMAEv2	-0.114	-0.329	-0.701

Table 7: RSI degradation slopes per occlusion family. All slopes have $R^2 > 0.82$.

Wilcoxon signed-rank tests. We compare V-JEPA 2.1 against each baseline across all nine occlusion \times severity cells. Differences from V-JEPA 2 and from VideoMAEv2 are statistically significant at $p < 0.01$. The comparison with VideoPrism is not significant in raw RSI, which is precisely the source of the decoupling discussed in the main section.

Reference	Baseline	N_{pairs}	$\bar{\Delta}$	W	p
V-JEPA 2.1	V-JEPA 2	9	+0.0155	45.0	1.95×10^{-3}
V-JEPA 2.1	VideoPrism	9	-0.0446	0.0	n.s.
V-JEPA 2.1	VideoMAEv2	9	+0.0616	45.0	1.95×10^{-3}

Table 8: One sided Wilcoxon signed-rank tests on per cell RSI differences.

CCR vs RSI decoupling. For each model and occlusion family we compute the decoupling index $DI = \mathbb{E}_s |\text{CCR}(s) - \text{RSI}(s)|$. A high DI means the classifier disagrees with itself even though the embedding is stable. VideoPrism has the largest DI under Patch Dropout because its RSI remains near 0.98 while CCR drops below 0.10. This is the quantitative form of the conclusion in the main section: representation stability does not imply decision stability.

Spatiotemporal Patch Dropout – The Pre-training Mirror
 3D cuboid patches zeroed ($\tau=2$ frames, $p=16px$). Directly mirrors V-JEPA 2 pre-training masking.

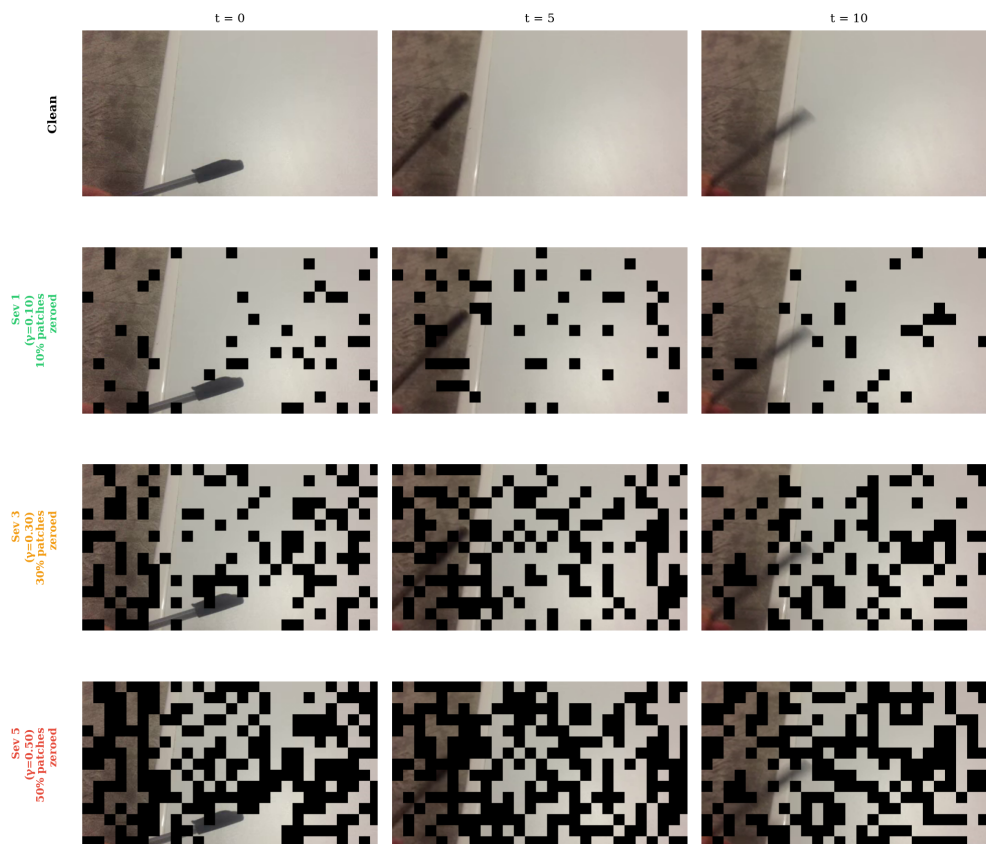


Figure 21: Spatiotemporal Patch Dropout. The volume is partitioned into 3D cuboids of size $(2, 16, 16)$ and a fraction γ are zeroed. This is the closest analogue at inference time to the masked patches used in V-JEPA pre-training.

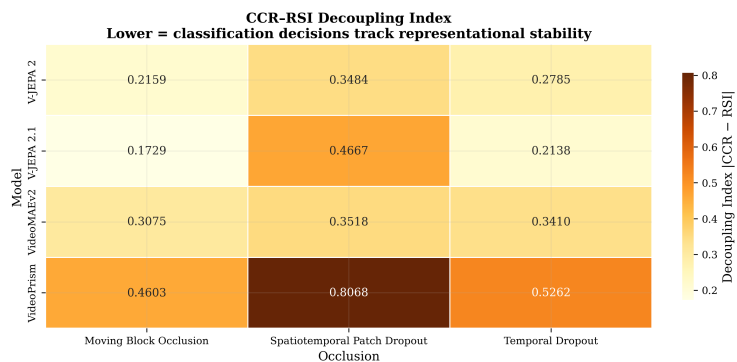


Figure 22: Decoupling index by model and occlusion type. VideoPrism shows the largest gap between RSI and CCR under Patch Dropout, despite having the highest raw RSI of any model.

Worst-case behaviour. For every encoder the worst case is Patch Dropout at severity 5. Table 9 reports CCR and probe Top-1 accuracy under this condition. The most stable encoder (VideoPrism) achieves the lowest accuracy, confirming the decoupling finding in the extreme case.

Table 9: Worst-case performance under Patch Dropout at severity 5.

Model	CCR (%)	Probe Top-1 (%)
V-JEPA 2.1	22.2	46.1
V-JEPA 2	40.9	16.8
VideoMAEv2	31.2	25.4
VideoPrism	7.2	2.7

F Temporal robustness: supplementary analysis

F.1 Experimental setup

We evaluate V-JEPA 2.1 (ViT-L), V-JEPA 2 (ViT-L), VideoPrism-Large, and VideoMAEv2-Large on a 1,000-clip subset of Something-Something v2 (174 classes, 16 frames per clip). Ten perturbation conditions span four families: *Permutation* (random shuffle, segment shuffle, interleaved reordering), *Static* (first, middle, or last frame repeated), *Noise* (Gaussian, uniform, temporally static Gaussian), and *Reversal*. Clean top-1 accuracies are 63.6%, 61.6%, 43.5%, and 20.6% respectively.

F.2 Frame permutation

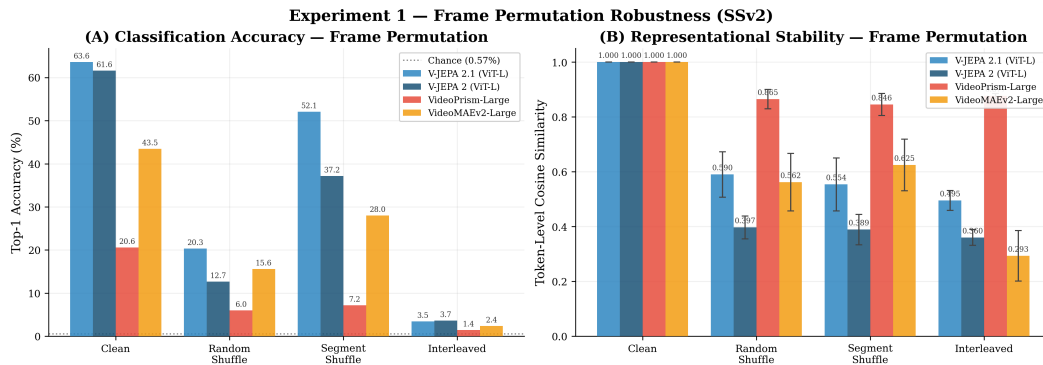


Figure 23: Classification accuracy and representational stability under three permutation granularities. Segment-level reordering is tolerated by all encoders; interleaving collapses both accuracy and cosine similarity for VideoMAEv2.

Figure 23 confirms the macro-versus-micro dissociation across all four encoders. Segment-level shuffling preserves coarse temporal context and retains moderate accuracy, whereas interleaving destroys it.

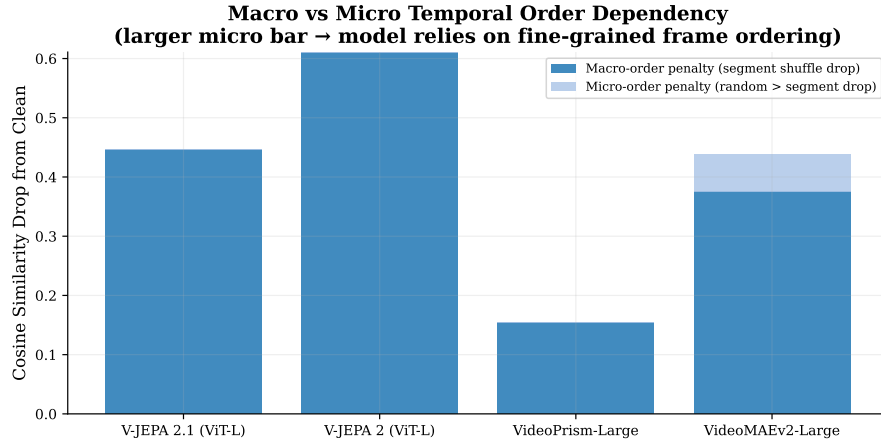


Figure 24: Decomposition of temporal order dependency into macro (segment shuffle drop) and micro (additional random shuffle drop) penalties. All models are predominantly sensitive to macro-level disruption.

Figure 24 decomposes the total cosine similarity drop into macro and micro penalties. The macro component dominates for every encoder, confirming that segment-level coherence, not frame-to-frame order, is the primary temporal cue.

F.3 Static video and spatial grounding

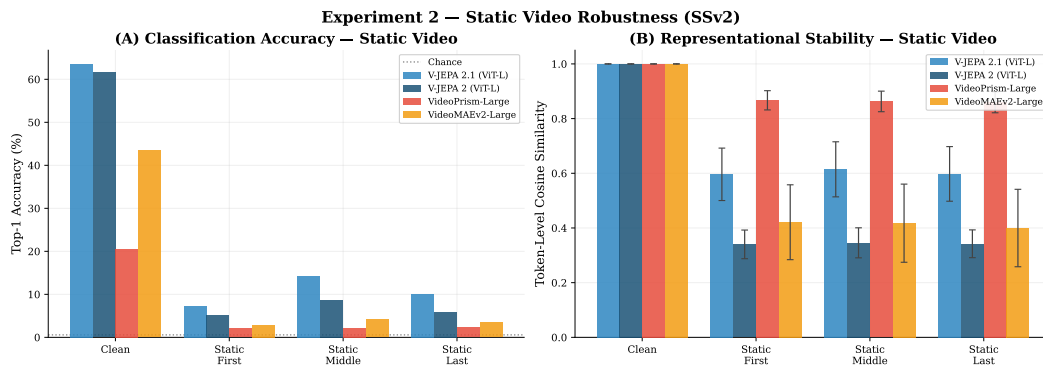


Figure 25: Accuracy and cosine similarity under single-frame static input. VideoPrism shows minimal representational change yet near-chance accuracy, confirming a spatial-only encoding.

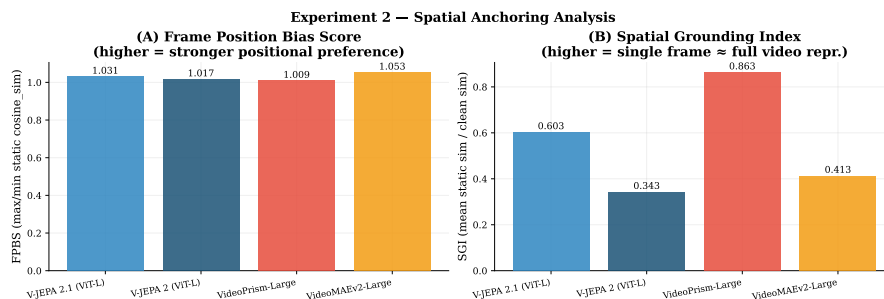


Figure 26: Frame Position Bias Score (left) and Spatial Grounding Index (right). V-JEPA 2.1 anchors to the middle frame; VideoMAEv2 and VideoPrism anchor to the first.

V-JEPA 2.1’s middle-frame anchoring (Figure 26) reflects a temporally integrative representation. VideoPrism’s SGI of 0.863 confirms that a single frame accounts for nearly all of its latent code.

F.4 Pure noise and temporal consistency

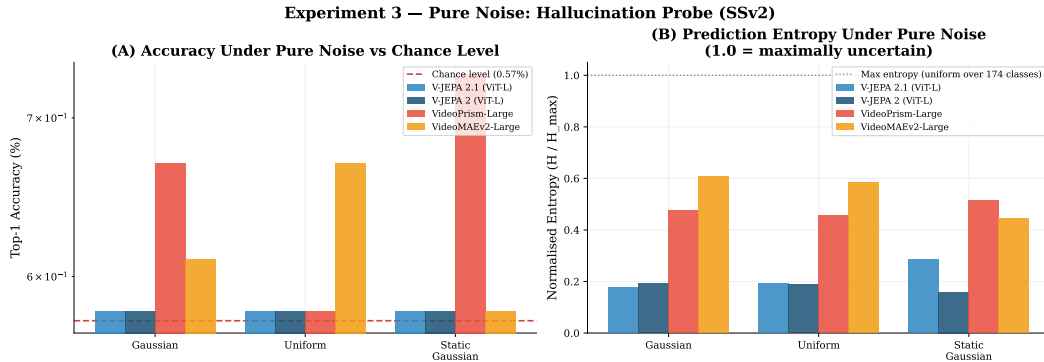


Figure 27: Accuracy and entropy under three noise types. All models fall to chance, ruling out semantic hallucination. Representational responses diverge sharply: VideoMAEv2 collapses to near-zero cosine similarity while VideoPrism’s remains above 0.77.

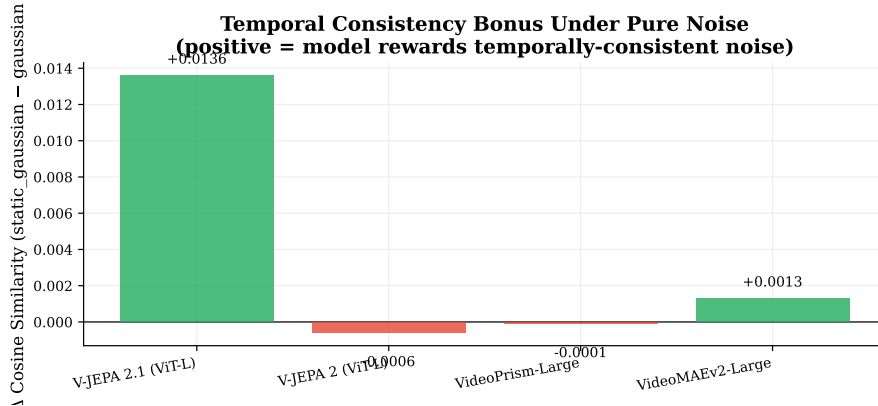


Figure 28: Temporal Consistency Bonus: difference in cosine similarity between temporally static and varying noise. V-JEPA 2.1 uniquely rewards frame-to-frame coherence even in the absence of semantic content.

V-JEPA 2.1 exhibits a positive temporal consistency bonus of +0.014 (Figure 28), indicating that its latent space actively rewards frame-to-frame coherence as a structural prior inherited from predictive pre-training. VideoPrism’s near-zero bonus reflects insensitivity to temporal structure. VideoMAEv2’s near-zero cosine similarity under noise (Figure 27) exposes fragility rather than temporal sensitivity.

E.5 Video reversal and directional coherence

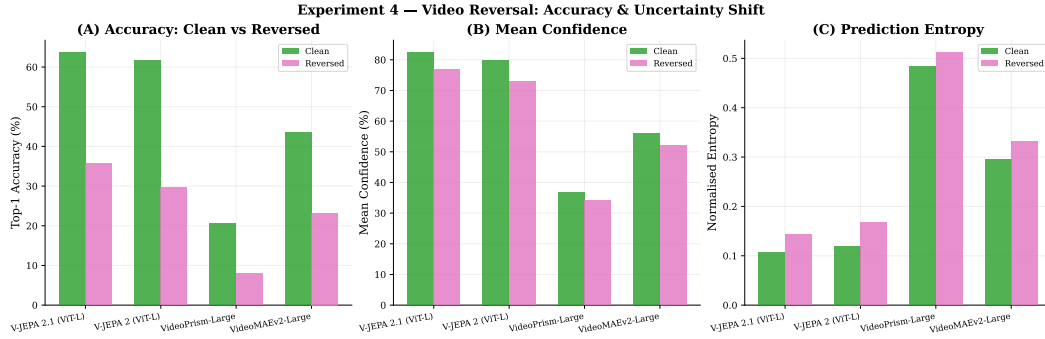


Figure 29: Accuracy, confidence, and entropy under video reversal. The V-JEPA models retain the highest accuracy; VideoPrism shows the largest entropy increase.

E.6 Temporal dependency index

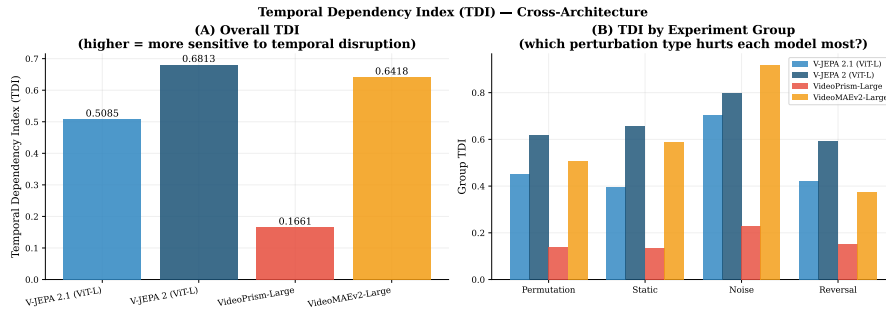


Figure 30: Temporal Dependency Index by perturbation family and overall. VideoPrism’s low TDI reflects insensitivity to temporal content, not robustness. VideoMAEv2’s high TDI reflects fragility under noise. V-JEPA 2.1 uniquely combines a moderate TDI with the highest accuracy.

The TDI ranks models as VideoPrism (0.17) < V-JEPA 2.1 (0.51) < VideoMAEv2 (0.64) < V-JEPA 2 (0.68). V-JEPA 2.1 occupies the only position that combines moderate temporal sensitivity with high classification accuracy (Figure 30). The TDI reduction from V-JEPA 2 to V-JEPA 2.1 alongside a 2-point accuracy gain suggests that iterative latent predictive pre-training converges toward representations that are both temporally grounded and resilient.

E.7 Cross-architecture summary

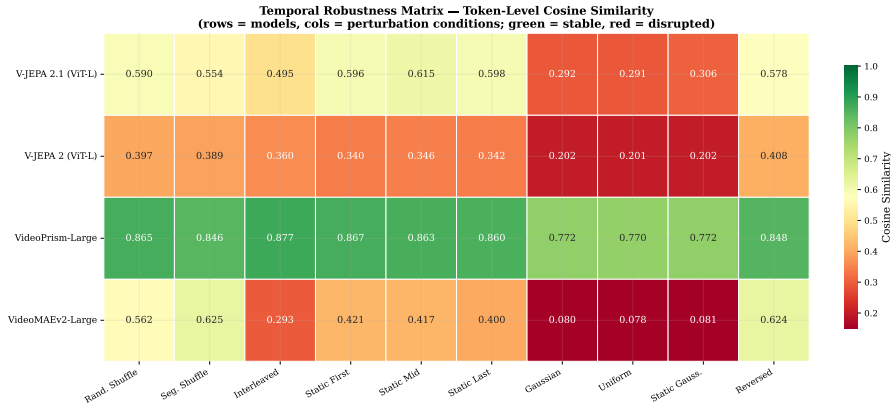


Figure 31: Full cross-architecture robustness heatmap. Green cells denote high cosine similarity (stable representation); red cells denote collapse. VideoPrism’s uniformly green row reflects spatial rigidity. VideoMAEv2’s red noise columns reflect fragility.

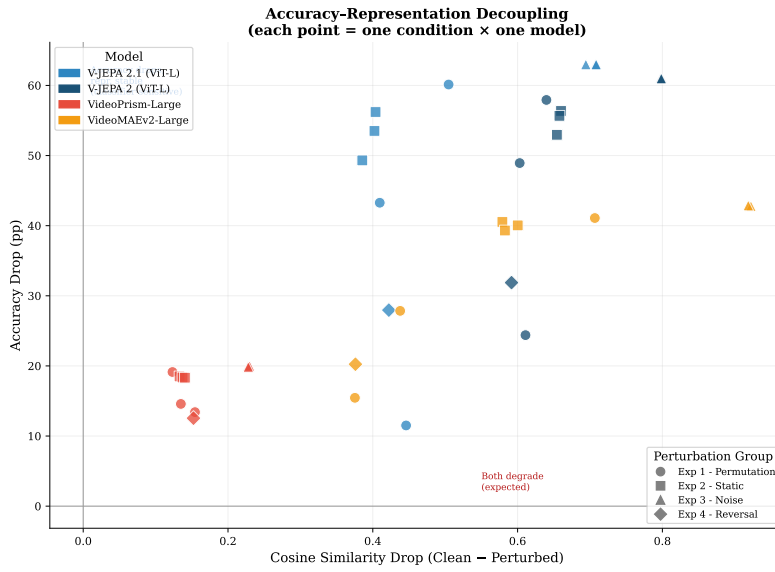


Figure 32: Accuracy drop versus cosine similarity drop across all conditions and models. VideoPrism clusters at low cosine drop but high accuracy drop, confirming that its stable representations do not support stable decisions.